Adsorption-desorption isotherms and x-ray diffraction of Ar condensed into a porous glass matrix

P. Huber and K. Knorr
Technische Physik, Universität des Saarlandes, D-66041 Saarbrücken, Germany
(Received 3 August 1998; revised manuscript received 16 April 1999)

Ar condensed into a porous glass matrix has been investigated by simultaneous measurements of adsorption-desorption isotherms and x-ray diffraction patterns as function of the pore filling above and below the melting point. The chemical-potential–temperature phase diagram has been established. It is consistent with a first-order phase transition between the adsorbate state and the capillary condensed state, above and below the melting temperature. The adsorbate and the capillary condensed state can also be distinguished in the diffraction patterns. A consistent picture of the structure and the thermodynamics is obtained.
[S0163-1829(99)09341-8]

I. INTRODUCTION

Porous glasses such as Vycor are permeated by an interconnected network of tubular channels. The diameters of the pores are in the nm range. A large variety of materials has been condensed into the pores, ranging from simple van der Waals systems, such as the rare gases,[1–3] to organic chain molecules,[4] semiconductors,[5] and metals.[6] Liquid metals have to be forced into the pores, as is standard for Hg porosimetry. Simple liquids are soaked into the ''thirsty'' glass and are obviously stable in the pore condensed state, at least as long as they do not solidify at lower temperatures. The adsorption isotherms of such liquids at low vapor pressures are similar to those obtained on planar substrates. At higher pressures a transition to complete pore filling is often observed which is due to capillary condensation. This situation has been called complete wetting in analogy to the terminology used for adsorbates on plane substrates. [For the case of incomplete wetting, the final thickness of the adsorbed layer on the walls when approaching the saturated vapor pressure $P_{\mathrm{sat}}(T)$ is less than the pore radius R.] The transition from the adsorbate state with a thin adsorbate layer covering the inner walls of the pores and vapor in the central part of the pores to the capillary condensed state is of first order and hence shows an intrinsic hysteresis on adsorption and desorption.[7] Figure 1 shows a schematic adsorption-desorption isotherm which is based on the idea of a mean-field first-order phase transition between the two states in a cylindrical pore of uniform diameter. At the pressure p_{coex} the two states are in equilibrium (see inset of Fig. 1), the upper and lower spinodal pressures p_u and p_l give the end points of the metastable sections of the adsorption and desorption branches. The variations of the pore diameter of the irregular pore network of porous glasses are expected to lead to a distribution of transition points which smear out the hysteresis and to pore blocking.[8] Note, however, that the first-order character of the transition and not pore blocking is the primary reason for the hysteresis. This is demonstrated by measurements on the matrix material MCM-41 which has practically uniform pores.[9]

The fundamentals of this transition have been worked out by Saam and Cole.[10] In contrast to adsorption on a planar substrate, two essential points have to be considered for adsorption on the inner walls of cylindrical tubes: (i) The area of the adsorbate-vapor interface decreases with increasing thickness of the adsorbed layer; thereby, the adsorbate-vapor surface tension enters into the problem. (ii) The adsorbate-substrate interaction potential is different from the planar case. In particular, the gradient of the potential vanishes in the center of the pore. The transition from the film state to the capillary condensed state occurs when the cost of adsorption energy related to the fact that molecules move farther away from the substrate equals the gain of interfacial energy related to the reduction of the vapor-condensate interface due to the formation of a concave meniscus. Thus, whenever the adsorbate layer grows to a thickness close to the pore radius, a phase transition will necessarily take place between the condensed film state and the filled pore state. The transition is of first order since it involves a fundamental change of the shape of the fluid-gas interface.

This model, complemented by assumptions on the distribution of the pore diameter, has been successfully fitted to adsorption isotherms of liquids in porous glasses. The model is confirmed by calculations based on the density functional approach.[7]

One wonders whether the same concept applies to solid pore condensates, whether solid condensates are at all stable in the pores. Dewetting transitions observed on cooling in some pore condensates suggest that this is not necessarily so.[11] In Sec. III A we will discuss this point on the basis of chemical potential μ vs temperature T phase diagrams which have been derived from adsorption isotherms above and below the melting point.

The confinement changes the properties of the material in the pores with respect to the bulk. Thus the melting and solidification temperatures T_m and T_s are both lower than in the bulk. The reduction ΔT is proportional to the inverse pore radius $1/R$.[12] The transition appears to evolve in a continuous way, but nevertheless shows considerable thermal hysteresis.[1] Several models have been proposed for these effects. Referring, for instance, to the standard nucleation model, solidification can only occur when T is lowered to such a point that the radius of the critical nucleus is smaller

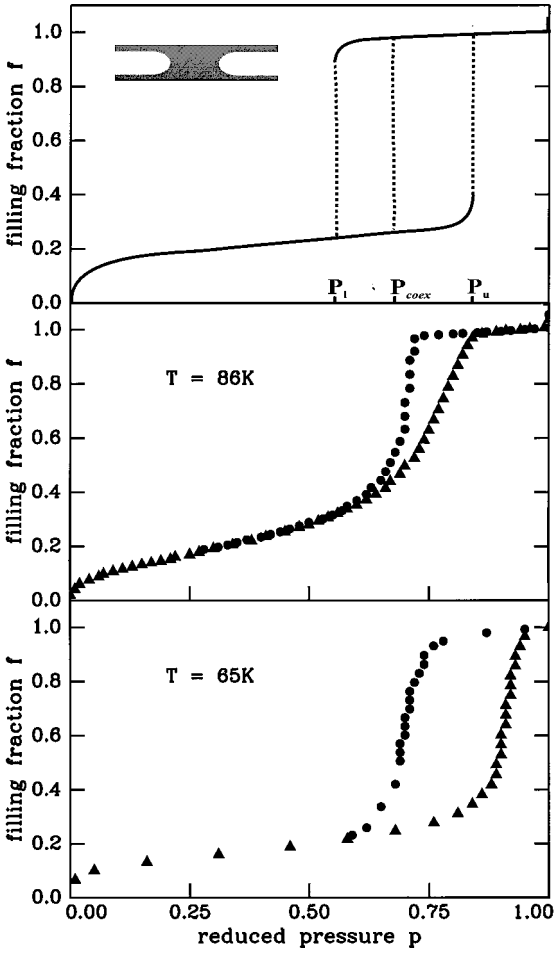

FIG. 1. Adsorption-desorption isotherms in the liquid state at 86 K and in the solid state at 65 K. A schematic isotherm as expected for a first-order phase transition between the adsorbate state and the capillary condensed state is shown in the top frame. The inset visualizes the coexistence of these two states in a capillary.

than the pore radius. Models of this type have been criticized for the reason that they refer exclusively to the geometrical confinement, but ignore the role played by the interaction with the substrate.[13] In fact, for strong adsorbate-substrate interactions one expects a layered structure of the pore condensate and a layerwise propagation of the boundary between the wall coating and the vapor. The multilayer phase diagrams of adsorbates on graphite (001) substrates give examples of this type.[14] The pore walls of the porous glasses form a heterogeneous substrate. The adsorption isotherms fail to show layering transitions. Hence the distinction of individual layers or shells is obscured; nevertheless, local probes can discriminate particles of the first and second layers from particles in the pore center.[15–17] The μ,T phase diagram resulting from our measurements will give also us insight into the melting of pore condensed Ar.

Diffraction studies on simple molecules such as H_2,[18] D_2,[19] Kr, Xe,[20] O_2,[21] and CO_2 (Ref. 22) in Vycor have revealed that the solidified capillary condensates are crystalline in the sense that some Bragg peaks, which are, of course, broadened due to finite-size effects, do exist in the diffraction patterns. On the other hand, the patterns are not identical to those of the bulk system. Solid H_2 was said to be crystalline, but neither hcp nor fcc. Recently, we have shown that the pattern of pore condensed N_2 can be quantitatively described as that of a hcp crystal with a tremendous amount of stacking faults.[23]

In Sec. III B we report diffraction results which elucidate the structure of the pore condensate, both in the adsorbate state at low fillings and in the capillary condensed state at higher fillings. We will also explain why we disagree with the interpretation of a recent x-ray diffraction study of Brown *et al.*[24] on Ar (and Kr) in Vycor according to which the solid pore condensates show a completely random stacking of spherical close-packed net planes just below the solidification temperature and transform at about 40 K into fcc crystallites which are still embedded in the porous matrix, but have sizes of at least 1000 Å.

II. EXPERIMENT

The porous glass used in this study is a controlled pore glass, ''Gelsil,'' a xerogel of almost pure SiO_2 with a nominal pore diameter of 75 Å as specified by the manufacturer (Geltech Inc., Orlando, FL). Our routine characterization of the matrix by N_2 adsorption at 77 K based on the Brunauer-Emmett-Teller (B.E.T.) analysis for the initial part of the isotherm and on the Kelvin equation for the vapor pressure necessary for emptying the pores shows that this matrix is similar to the standard Vycor glass (No. 7930), but has a somewhat larger porosity.[17] For comparison, we will also show some diffraction data obtained on standard Vycor glass, on another type of Vycor glass with a pore diameter of 130 Å, and on a xerogel with 25 Å.

The experimental setup allows the simultaneous measurements of volumetric adsorption isotherms and x-ray diffraction patterns. A tablet of the porous glass substrate (0.3 g) is mounted in a copper sample cell. The cell is equipped with two Be windows for the passage of the incoming and outgoing x-ray beams. The cell is attached to the cold plate of a closed-cycle refrigerator. Temperatures above and below the bulk triple point ($T_3^{\mathrm{bulk}}=83.8\,\mathrm{K}$) have been investigated. The temperatures are stabilized to better than 0.05 K. A capillary connects the cell to an all-metal gas handling system at room temperature. The vapor pressure P is measured with capacitive membrane gauges of 10 and 1000 mbar full scale. The thermodynamic state of the pore condensed material will be given in terms of the variables temperature T, reduced pressure $p=P/P_{\mathrm{sat}}$, and filling fraction $f=N/N_0$. $P_{\mathrm{sat}}(T)$ is the saturated vapor pressure of bulk Ar, N the number of Ar particles in the cell, and N_0 the number necessary for the complete filling of the pores. N_0 is about 12 mmol. At T_3^{bulk} the vapor in the dead volume of the cell and the gas handling system is of the order of 1 mmol. The use of reduced quantities for the pressure and the amount of material minimizes the effect of systematic errors. Thus one can safely ignore the effect of the temperature difference between the sample and the gauge on the reduced pressure p.

For the x-ray powder diffraction experiment the Bragg-Brentano configuration has been chosen. The radiation comes from a rotating Cu anode operating at 10 kW and is monochromatized by reflection from a graphite (002) crystal ($\lambda=1.542\,\mathrm{Å}$). The diffraction patterns cover scattering angles 2θ from 15° to 65°. All features observed in the

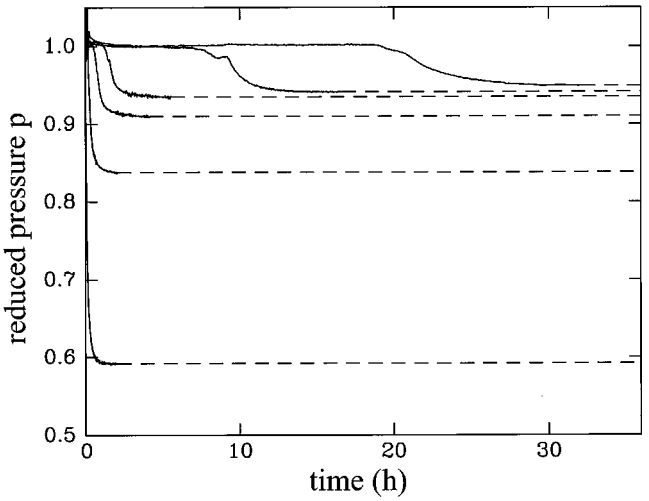

FIG. 2. The approach of the reduced pressure to equilibrium for some data points of the adsorption branch of the 65 K isotherm of Fig. 1. The f values from bottom to top are 0.23, 0.32, 0.45, 0.6, 0.85, and 0.93. The saturated vapor pressure (corresponding to $p=1$) is 26.3 mbar.

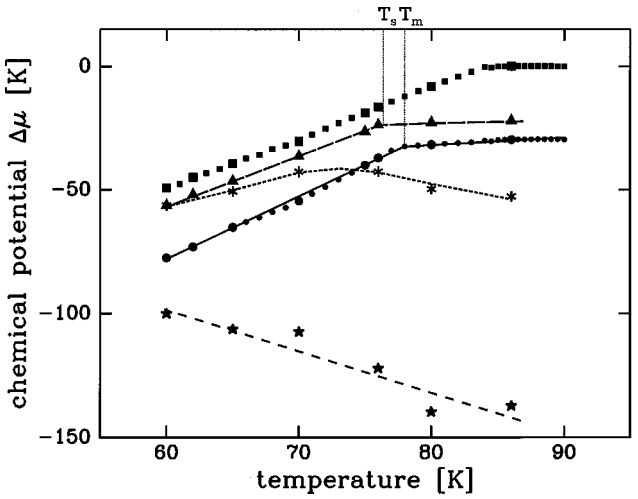

FIG. 3. The difference of chemical potential for various states of the adsorption-desorption isotherms with respect to the bulk liquid: squares, $p=1$, the bulk vapor pressure; triangles, μ_a, capillary condensation on adsorption; circles, μ_d, pore emptying on desorption; asterisks, μ for $f=0.3$ (equivalent to two monolayers) on adsorption; stars, μ for $f=0.15$ (equivalent to one monolayer).

patterns of the pore condensate exceed the instrumental 2θ resolution by far. Hence resolution effects can be ignored.

III. RESULTS AND DISCUSSION

A. Thermodynamics

In total seven adsorption-desorption isotherms have been measured. Figure 1 shows one isotherm of the liquid state ($T=86$ K) and one of the solid state ($T=65$ K) of the pore condensate. For the measurement of an isotherm small portions of gas are consecutively introduced into the cell and the pressure is allowed to relax towards equilibrium in each step. The equilibration time increases with decreasing T and with p approaching 1. Figure 2 shows the time dependence of the vapor pressure for several data points of the adsorption branch of the 65 K isotherm. As can be seen in the figure, the relaxation can be extremely slow with intermediate long-lived instable states. The most prominent intermediate state is $p=1$; here, the extra material offered to the substrate obviously forms bulk crystallites outside the pores first and enters into the pores via distillation only afterwards. The intermediate states with $p<1$ remain unexplained; perhaps, they are related to temporary pore blocking. At 60 K equilibration times of several days have been observed. It is clear that the intermediate instable state at $p=1$ occurring in the final part of the adsorption branch can be easily misinterpreted as incomplete wetting.

The initial part of the isotherms is similar to what is obtained for physisorption on planar heterogeneous substrates. There are no steps due to layering transitions. At higher p, a clear hysteresis between adsorption and desorption shows up. This type of behavior is well known from experiments on a large number of liquids in porous substrates. We use the point of steepest ascent on adsorption and of steepest descent on desorption to define the characteristic pressures p_a and p_d. The final change of the isotherm from horizontal to vertical defines $p=1, f=1$. For $f>1$, bulk material condenses outside the pores at $p=1$.

The characteristic pressures of the isotherms $p_d, p_a, p=1$ and additionally the pressures at $f=0.15$ and $f=0.30$ (of the adsorption branch), which according to the B.E.T. analysis correspond to wall coatings of, respectively, one and two monolayers, have been converted into the chemical potential $\Delta\mu=\mu-\mu^{\mathrm{bulk}}=k_BT\ln(p)$. Figure 3 shows the μ-T phase diagram. Here the chemical potential of the bulk liquid for $T>T_3^{\mathrm{bulk}}$ and its linear extrapolation to temperatures below T_3^{bulk} is used as the origin of the μ scale. Data points derived directly from the isotherms are indicated in Fig. 3 by bigger symbols. The other data points, on $p=1$ and p_d, have been obtained from heating scans on fixed amounts of gas enclosed in the cell. In such heating scans—and in an analogous way also in cooling scans—the amount of condensed material f and the reduced pressure p are not strictly constant because of evaporation (=desorption) of the condensate into the dead volume or condensation (= adsorption) of the vapor out of the dead volume into the pores. The corrections can be estimated and turn out to be negligible in all instances where we refer to such quasi-isosteric data.

Although this is not of direct importance for the interpretation, we suggest to relate the filling pressure p_a of the experiment to the upper spinodal pressure p_u of the mean-field model described in the Introduction. The emptying pressure p_d is presumably closer to p_{coex} than to the lower spinodal pressure p_l. Note that even in the completely filled state, the condensate in every capillary terminates at the external surface of the porous glass sample with a meniscus. On desorption the pores simply empty by a retreat of the meniscus, which just means $p_d=p_{\mathrm{coex}}$. p_l would be relevant in the unrealistic case of a closed pore where the meniscus had to be created as the necessary first step toward emptying.

The variations of the characteristic pressures with temperature are best discussed in terms of the μ-T diagram (Fig. 3). The T variation of the μ^{bulk} is in agreement with the literature. The kink at about 84 K defines T_3^{bulk}. The enthalpy of fusion H^{bulk}, $H^{\mathrm{bulk}}=T_3^{\mathrm{bulk}}\Delta S$, as obtained from the differ-

ence of the slopes ($\partial\mu/\partial T=-S$) above and below T_3^{bulk} is $(1300\pm100)\,\text{J mol}^{-1}$, in agreement with the literature. $\mu_d(T)$ and $\mu_a(T)$ are both smaller than $\mu^{\text{bulk}}(T)$ throughout the T range investigated. Thus the pore condensate is stable with respect to the formation of bulk droplets or crystallites outside the pores. Note, however, that the difference with the bulk is small, of the order of a few K with respect to both T and μ.

The kink of $\mu_d(T)$ at about 78 K defines the transition from the solid to the liquid state of the capillary condensed material, which is relevant if the system is held on the desorption branch, as is the case for quasi-isosteric heating. We will therefore refer to this temperature as the melting temperature T_m. Calculating the point of intersection of the low-T section with the high-T section of $\mu_d(T)$, one arrives at the following relation for T_m:

$$T_3^{\text{bulk}}-T_m=(\Delta\mu_d^{\text{liq}}-\Delta\mu_d^{\text{solid}})/\Delta S.$$

$\Delta\mu_d^{\text{liq}}$ and $\Delta\mu_d^{\text{solid}}$ are the differences between μ_d and μ^{bulk} in the solid and liquid states at $T=T_3^{\text{bulk}}$, respectively. (Here and in the following $\Delta\mu$'s are always defined as positive quantities.) The values of $\Delta\mu_d^{\text{liq}}$ and $\Delta\mu_d^{\text{solid}}$ are directly accessible from Fig. 3 by linear interpolation and extrapolation, respectively, of the high-T and low-T sections of $\mu_d(T)$. One arrives at a value of (78.0 ± 0.3) K for T_m. Note that the entropy of the capillary condensate, as obtained from the slope of $\mu_d(T)$, is slightly lower than for the bulk, for both the liquid and solid states. The enthalpy of melting of the pore condensate, H_m, as obtained from the difference of the slopes of $\mu_d(T)$ above and below T_m, is, however, within experimental error identical to H^{bulk}.

The same reasoning can be applied to the adsorption branch, represented by $\mu_a(T)$. We define the temperature T_S of the intersection of the low-T and high-T linear sections of $\mu_a(T)$: $T_S=(76.2\pm0.5)$ K. T_S is related to the quantities $\Delta\mu_a^{\text{liq}}$ and $\Delta\mu_a^{\text{solid}}$ by an expression analogous to that given above for T_m. T_S is the temperature of the liquid-solid transition when the system is held on the adsorption branch. This is the case for solidification in a quasi-isosteric cooling scan. The slopes of $\mu_a(T)$ above and below T_S are within experimental error identical to their bulk counterparts.

Combining the expressions for T_m and T_S gives

$$T_m-T_S=(\Delta\mu_{a\text{-}d}^{\text{solid}}-\Delta\mu_{a\text{-}d}^{\text{liq}})/\Delta S.$$

$\Delta\mu_{a\text{-}d}^{\text{solid}}$ and $\Delta\mu_{a\text{-}d}^{\text{liq}}$ are the widths of the hysteresis of the adsorption-desorption isotherms, expressed as differences of chemical potentials, of the solid and liquid states of the pore condensate. An inspection of Fig. 3 and of the two isotherms of Fig. 1 clearly shows that $\Delta\mu_{a\text{-}d}^{\text{solid}}>\Delta\mu_{a\text{-}d}^{\text{liq}}$ and that accordingly there should be a finite thermal hysteresis of solidification and melting. Further, below, the temperatures T_m and T_S of the μ-T diagram will be compared with the melting and solidification temperatures of diffraction measurements obtained in the course of a quasi-isosteric heating and cooling scan.

We summarize: The depression of T_m and T_S relative to T_3^{bulk} is due to the fact that the difference of the chemical potential with respect to the bulk system is smaller in the solid than in the liquid state. The solid and liquid pore condensates are both stabilized by the interaction with the glass matrix, but the liquid state profits more from the attractive potential of the substrate than the solid. T_S and T_m are directly related to $\mu_a(T)$ and $\mu_d(T)$, as shown by the μ-T phase diagram and by the expressions for T_S and T_m. The thermal hysteresis between solidification and melting in quasi-isosteric runs and the adsorption-desorption hysteresis of the isotherms are also directly related. Both types of hysteretic behavior refer to the same reservoir of metastable states, namely, those lying between $\mu_a(T)$ and $\mu_d(T)$ in the μ-T plane.

As just pointed out, the reduction of T_S and T_m relative to T_3^{bulk} is due to the fact that $\Delta\mu_i^{\text{liq}}>\Delta\mu_i^{\text{solid}}, i=a,d$. Can the model of Saam and Cole account for the changes of the $\Delta\mu$'s upon solidification? The parameters of the model are the strength of the molecule-substrate interaction α_{ms} and the product σv of the condensate-vapor interfacial energy and the molar volume of the condensate. We have calculated the characteristic pressures p_m ($=p_{\text{coex}}$; see Fig. 1) and p_c ($=p_u$) of the model for a homogeneous pore with $D=75$ Å. We identify the pressures p_m and p_c with the pressures p_d and p_a of our experiment. In the liquid state at $T=86$ K (Fig. 1) one arrives at a reasonable agreement with the experiment ($p_d=0.70$, $p_a=0.78$, $p_m=0.70$, $p_c=0.79$) by using literature values[25] for σ and v, $\sigma=11.86\times10^3$ N/m, $v=28.36\times10^{-6}\,\text{m}^3$, and by setting α_{ms} to 0.5 eV Å^3. There is, however, no way to reconcile the model and experiment in the solid state. We refer, for instance, to the value of p_d at 65 K, which is again 0.70. The model can reproduce this value by reducing the parameter σv by about 28% while leaving α_{ms} unchanged. The value resulting for p_c is 0.80, in contradiction to the experimental value of p_a of 0.91. Thus it is in particular the increased width of the adsorption-desorption hysteresis of the solid state where the model fails. Hence the model needs to be refined, preferentially by a more microscopic view of the adsorbate-adsorbate interaction. Further, below, we will propose that the reduced stability of the pore solid with respect to the pore liquid is not so much due to a reduced surface tension σ, but to a large number of lattice faults.

Nevertheless, one should keep in mind that the solidified pore condensate is still stable with respect to the bulk system. Obviously, it profits from the attractive adsorbate-substrate potential. In order to do so, the pore solid must nestle against the walls and form a concave meniscus, similar to the liquid. A smooth meniscus can be realized above the roughening temperature, only. Estimates based on the layer critical points of Ar multilayers adsorbed on graphite suggest a roughening temperature of the (111) surface of fcc Ar of the order of 68 K.[29] Our study extends to temperatures well below this value without showing any evidence for a change of the thermodynamic behavior, let alone an indication of a dewetting transition. Clearly, the concept of a meniscus becomes debatable in pores with diameters of some tens of Å and a microscopic or at least layerwise model would be more appropriate.

The μ-T phase diagram of Fig. 3 also includes data on the chemical potential for lower fractional fillings, namely, $f=0.15$ and $f=0.30$, which roughly correspond to one and two monolayers, respectively. The relatively large scatter of these data results from the fact that the adsorption isotherms

are close to horizontal at these low fillings. The results show that the entropy of these layers is larger than for bulk solid and even for the bulk liquid. This is quite common for adsorbates on planar substrates and leads to a delayering transition at the temperature where the layer line intersects the $\mu^{\text{bulk}}(T)$ curve. In the present case the intersections with the capillary condensation lines $\mu_a(T)$ and $\mu_d(T)$ are of more interest. $\mu(T)|_{f=0.30}$ approaches $\mu_a(T)$ at about 60 K, which means that below 60 K capillary condensation is induced by a wall coating of less than two monolayers. The corresponding extrapolated temperature for the first monolayer is of the order of 50 K.

Do the first and second layers undergo a melting transition? The gradual change of slope of $\mu(T)|_{f=0.30}$ around 70 K may suggest this for the second layer. There is, however, no clear indication for a melting transition of the first monolayer. This would be consistent with the idea that the molecules of the first layer are immobile because of the heterogeneous nature of the substrate which is responsible for a substantial corrugation of the adsorption potential. On the other hand, we cannot exclude that the melting of the first monolayer takes place below 60 K.

At the end of this section we want to discuss a pitfall of experiments on pore condensates, namely, the formation of the bulk solid under nonequilibrium conditions. Note that according to Fig. 3 the difference $\Delta\mu_a=\mu^{\text{bulk}}-\mu_a$ for the solid regime is of the order of 5 K, only. Due to its low thermal conductivity and possibly a bad thermal contact to the metal walls of the cell, the temperature of the glass matrix lags upon temperature changes. For fast cooling or heating, distillation occurs. Rapid cooling transfers the material out of the pores onto the colder walls, subsequent heating reverses the process, and a layer of bulk solid is formed on the external surface of the glass tablet. This is in fact how we prepared the bulk layer, the diffraction pattern of which is shown in the top frame of Fig. 4. Practically any desired partition of capillary condensate and bulk solid can be produced with this technique.

The effects are more subtle in case the cooling rate is slow enough that the temperatures of the glass and cell are equilibrated. Nevertheless, there is a net transfer of particles from the vapor to the condensate on cooling. The relaxation time of this process can be estimated from the equilibration time of isothermal adsorption (Fig. 2) and $\Delta\mu_a$. For 65 K one arrives at a maximum tolerable cooling rate of the order of 5 K per 30 h. Faster cooling inevitably leads to a nonequilibrium state in which the residual vapor in the dead volume condenses (at $p=1$) into parasitic bulk crystallites outside the glass matrix. In principle, quasi-isosteric heating and cooling are a legitimate way of changing the thermodynamic state of the pore condensate, but it requires a careful control of the vapor pressure and of the amount of material remaining in the pores. The formation of bulk crystallites at $p=1$ may simply be a nonequilibrium effect rather than a dewetting transition.

We think that the sharp fcc diffraction peaks observed by Brown *et al.*[24] below 40 K are due to such bulk crystallites. Of course, we do not know the details of this experiment, but obviously the vapor pressure has not been recorded. Furthermore, we cannot imagine that the limited beam time at a synchrotron source allows cooling rates as slow as those estimated above. We are also sceptic about the thermometry of this study. The quoted T_S value of 64 K for Ar in Vycor is more than 10 K lower compared to what we and others[1] observe.

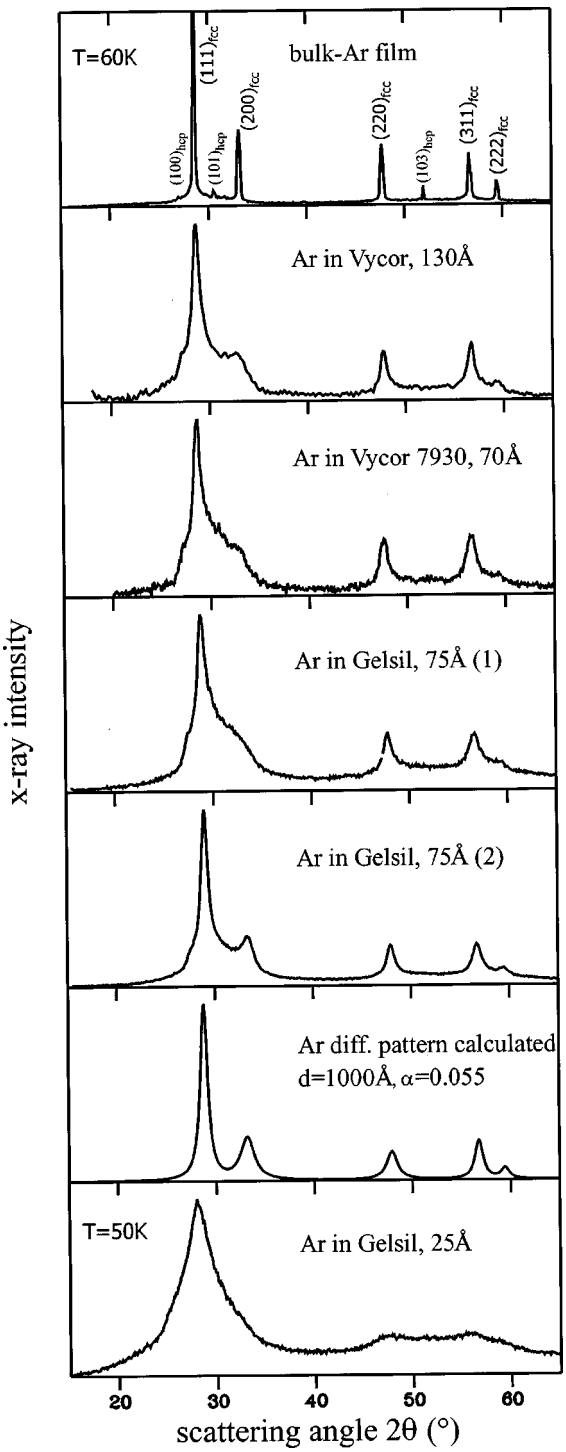

FIG. 4. Diffraction patterns of a bulk Ar film and Ar pore condensates in porous glasses with various pore diameters. For the xerogel Gelsil 75 Å, pattern (2) is obtained from capillary condensation in the solid state, pattern (1) from capillary condensation in the liquid state and subsequent solidification by cooling. All patterns are for practically completely filled pores. The temperature is 60 K, except for the 50 K pattern of the condensate in the 25 Å pores. Also shown is a calculated pattern considering finite size and stacking faults.

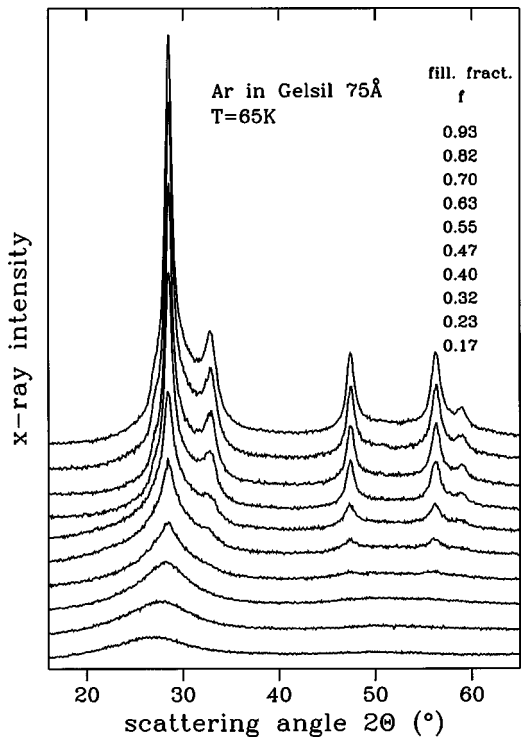

FIG. 5. The evolution of the diffraction pattern in the solid state at 65 K with fractional filling.

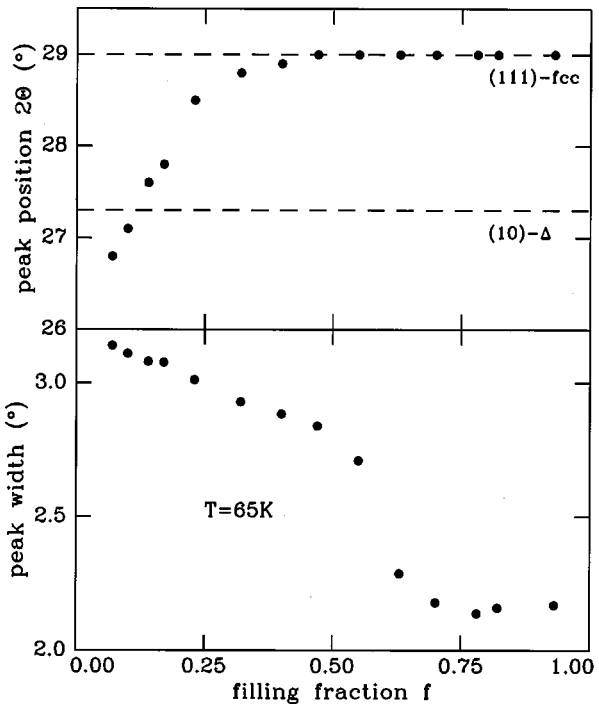

FIG. 6. The position and width of the first maximum of the diffraction pattern, which develops into the (111) peak, as function of f at 65 K. The upper dashed line marks the (111) position of the bulk solid, the lower dashed line the (10) position of a triangular lattice having the same next-neighbor distance.

B. Structure

Diffraction patterns have been recorded in parallel with the adsorption isotherms, that is, at constant T as function of f and occasionally also as function of T in quasi-isosteric runs. As far as the position of the first maximum of the liquid structure factor is concerned, there are no detectable differences to liquid bulk Ar. We concentrate on the solidified pore condensate and start at a temperature well below the solidification. Figure 4 shows diffraction patterns of the solid material in several types of porous glass for almost complete filling. In all diffraction patterns the contribution of the substrate has been subtracted, properly accounting for the f-dependent absorption of the x rays. The figure also includes a pattern on an evaporated bulk Ar film for comparison. The bulk film shows a minority hcp component, with an ideal c/a ratio and a next-neighbor distance identical to that of the fcc majority component.

Pore condensed solid Ar shows the reflections expected for a fcc solid. The width of the peaks increases with decreasing pore diameter. For the matrix with the smallest pore diameter, namely, 25 Å, the (200) and (222) reflections are practically absent. The patterns of the pore solid in the 75 Å xerogel and in the standard Vycor glass suggest that these two matrices are very similar, apart from the higher porosity of the xerogel. This leads to a superior quality of the patterns obtained with the xerogel. The patterns depend on the way of preparation of the pore condensate. For pattern (2) the condensate has been adsorbed and the capillary condensed in the solid state, whereas for pattern (1) the material has been condensed in the liquid state and solidified by cooling. Obviously, the former method warrants a better sample quality with sharper diffraction peaks.

Figure 5 shows diffraction patterns for $0.17<f<0.93$ of the adsorption branch of the 65 K isotherm. At low f, $f<0.3$, that is, for a coating of the walls with less than two monolayers, the diffraction patterns show two broad maxima, the first one centered at $2\theta=27°$ and the second one extending from about 45° to 58°. Altogether, the patterns suggest that these thin layers are highly disordered, amorphous. Further insight comes from a comparison to monolayers on planar homogeneous substrates such as graphite. Here Ar monolayers form a close-packed triangular lattice, similar to the (111) plane of the bulk fcc crystal.[27] We have calculated the powder diffraction patterns of such a two-dimensional planar array[26] and arrive at a satisfactory fit of the $f=0.17$ pattern by choosing a coherence length of the order of 16 Å. The first maximum is identified as the (10) peak, the second as strongly broadened, overlapping (11) and (20) reflections. The next-neighbor distance d_{nn}, as calculated from the (10) position, is close to the value obtained from the positions of the fcc Bragg peaks at high f. For the lowest filling fraction, d_{nn} is slightly enlarged (Fig. 6). This effect is presumably due to the heterogeneous character of the substrate, which does not allow a perfectly close triangular packing.

The diffraction patterns change smoothly from the amorphous type at low f to the quasi-fcc type at high f. This is consistent with the smooth, rather than stepped, shape of the adsorption isotherm. Nevertheless, Figs. 5 and 6 shows some conspicuous changes of the patterns with increasing f. We try to localize these changes by inspecting the fcc reflections (111), (200), and (220). These reflections respond quite differently to the number and to the stacking sequence of close-packed triangular planes. Examples have been calculated in context with diffraction measurements on Ar multilayers ad-

sorbed on a homogeneous graphite substrate.[27] The (111) reflection develops out of the triangular (10) reflection, a process which involves a shift of the peak position. The final position is reached at $f=0.45$, which corresponds to about three monolayers (Fig. 6). The reflection is common to all close-packed stacking sequences, such as fcc *ABC* or hcp *AB*. The width of the (111) reflection decreases with an increasing number of stacked planes. The drop of the width around $f=0.60$ (Fig. 6) is therefore due to an increase of the number of stacked planes. The (200) reflection is specific to fcc *ABC* stacking and does not have a counterpart in two dimensions. The (200) reflection becomes visible at $f=0.47$. The (220) reflection is the successor of the (11) reflection of the triangular lattice. The (220) reflection can be identified as a sharp feature at $f=0.40$ and above. We suggest that the changes of the diffraction pattern are due to the onset of capillary condensation. The most reliable estimate for the critical value f_C is presumably 0.40. This value compares favorably with the adsorption branch of the 65 K isotherm of Fig. 1. The somewhat larger value extracted from the (111) width results from the fact that here the broad peak of the adsorbate and the sharper peak of the capillary condensate superimpose, the intensity of the latter increasing in proportion to $f-f_C$. As suggested by the f dependence of the (111) position, the principle of close packing appears to be obeyed already in the adsorbate state with a film thickness as low as three monolayers. The somewhat delayed appearance of the (200) reflection may arise from the fact that the capillary condensation starts in the narrow sections of the pores. Here deviations from the fcc stacking sequence *ABC* are particularly likely.

In the following we concentrate on the quasi-fcc-type component of the patterns representing the capillary condensed pore solid, which is obtained by subtracting the adsorbate component, represented by the pattern at $f=0.40$, from the $f=0.93$ pattern. Analogous to our interpretation of the diffraction pattern of pore condensed hcp N_2, we consider two line broadening effects: the finite size d of the crystallites and stacking faults.[28] α is the probability that an *AB* stack of (111) planes is followed by a plane in the *A* position rather than in the *C* position. Figure 4 includes a simulated pattern with $d=1000$ Å and $\alpha=0.055$. This choice of parameters describes the difference pattern quite well, in spite of the simplicity of the model. The value of d exceeds the pore diameter by far; this points to a rather large coherence length along the pore. One is inclined to identify d with average chord length of a curved pore. There is an additional feature in the patterns at higher f (Figs. 4 and 5), namely, a shoulder on the low 2θ wing of the (111) peak which is not accounted for by the model, but which is nevertheless related to stacking faults. The position of the shoulder coincides with the (100) peak of the metastable hcp phase of Ar. For a random stacking of the net planes, the diffracted intensity appears on a triangular array of Bragg rods perpendicular to the (111) plane. The minimum 2θ value of the (10) rod coincides with the Bragg angle of $(100)_{\mathrm{hcp}}$. Thus the shoulder is another piece of evidence for a large density of stacking faults.

It appears that the solid condensate adapts to the restricted geometry in the pores by the formation of stacking faults and presumably other lattice faults which are not considered in our model. The energy of these lattice defects causes an increase of the chemical potential of the solid pore condensate, thereby reducing the difference of the chemical potential with respect to the bulk solid (which in turn leads to a lowering of the melting point). The same idea has been mentioned in connection with the pressure-induced solidification of He in fine powders.[30]

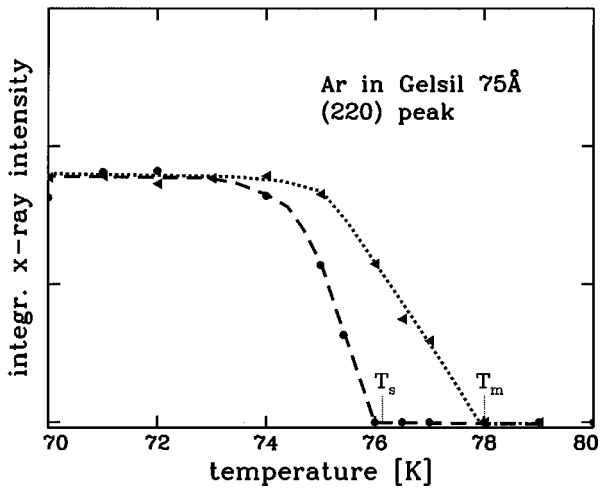

FIG. 7. The T dependence of the intensity of the (220) peak in the melting region on quasi-isosteric cooling and heating for $f=0.8$. The melting and solidification temperatures of the μ-T diagram, T_m and T_S, are indicated for comparison.

Figure 7 shows the integrated intensity of the (220) peak for a quasi-isosteric cooling and heating scan. The appearance of the peak on cooling signals crystallization, the disappearance on heating melting. One notes a thermal hysteresis of the order of 1–2 K, and solid-liquid coexistence regions both for cooling and heating in which the peak intensity varies with T in a roughly linear fashion. Both observations are in qualitative agreement with heat capacity and ultrasonic measurements on Ar in Vycor.[1] We define the solidification and melting temperatures of the quasi-isosteric scans, T_S^{qi} and T_m^{qi}, as the high-T end points or alternatively as the midpoints of the coexistence regions. The values obtained for the former case, 76 and 78 K, agree quite well with the temperatures $T_S=(76.2\pm0.5)$ K and $T_m=(78\pm0.3)$ K extracted from the μ-T phase diagram. The values for the latter case are 75.5 and 76.5 K. Here the agreement is not satisfactory.

For temperatures T, $T_S<T<T_m$, the μ-T the phase diagram suggests that the pore condensate of the adsorption branch with the chemical potential μ_a is still liquid, but that the condensate of the desorption branch with the chemical potential μ_d is already solid. Thus it should be possible to control the structural state of the pore condensate by adsorption and desorption. Pertinent diffraction results exist for 76 K (Fig. 8). Note that this temperature is just outside the thermal solidification-melting hysteresis when referring to the temperatures T_S and T_m of the μ-T diagram, but inside in terms of T_S^{qi} and T_m^{qi} of Fig. 7. Indeed, the diffraction patterns at 76 K (Fig. 8) show that upon adsorption the diffraction patterns are of the amorphous or liquid type. The fcc reflections appear only close to complete filling, above $f=0.9$. (As has been discussed in Sec. III A, the critical value f_C of

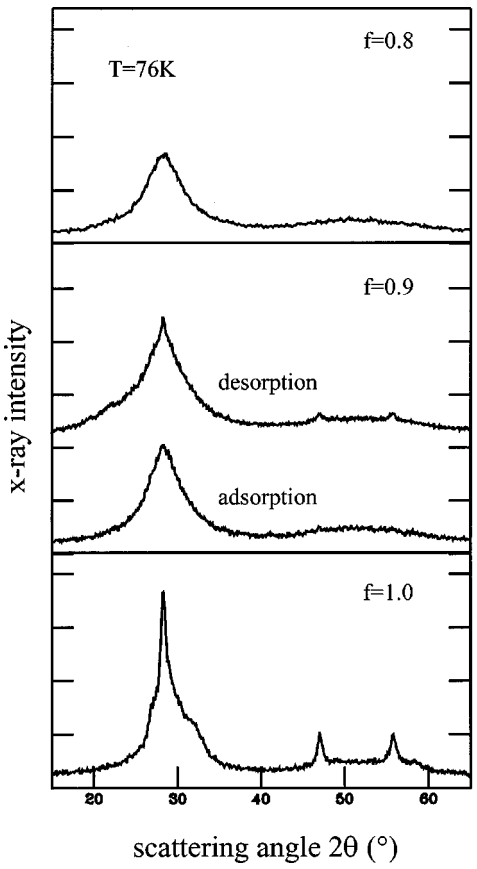

FIG. 8. Diffraction patterns at $T=76$ K, i.e., at a temperature intermediate to melting and solidification. Note that for $f=0.9$, the peaks of quasi-fcc material are visible on desorption, but not on adsorption.

capillary condensation increases with T.) On desorption, however, remainders of the fcc reflections are still present at $f=0.9$ and extrapolate to zero at about $f=0.8$.

One wonders whether the capillary condensate forms on top of the adsorbed layers or whether the capillary condensation leads to a reorganization of the material on the pore walls. The patterns of the adsorption branch of Fig. 8 show that the growth of the fcc peaks between $f=0.9$ and $f=1$ is connected with a decrease of the amorphous component. See the 2θ range left of the (111) peak. The analysis of these changes suggests that half of the adsorbate, two out of four monolayers, takes part in the crystallization process of the capillary condensate. It is natural to think of the third and fourth layers, which means that the first and second layers remain in the original state. The recrystallization of the higher layers of the film state can be only observed at higher temperatures since at lower temperatures, of the order of 60 K, the capillary condensation starts already when the wall coating has reached two monolayers. As far as the hypothetical melting of the first and second monolayers is concerned, the diffraction pattern cannot really decide whether these layers are liquids or amorphous solids. Altogether, the diffraction results are in agreement with the conclusions drawn from the thermodynamic data and given further insight into the structural organization of the pore condensate.

Brown *et al.*[24] interpret the diffraction patterns of pore condensed Ar at 55 K and of Kr at 94 K in Vycor ($f\approx0.9$) in terms of a disordered hexagonal close-packed structure with random stacking of net planes. However, the patterns of Brown *et al.* clearly show a residual (200) intensity having the form of a shoulder. Analyzing these patterns, we arrive at estimates of stacking fault probability α of around 0.2. This is larger than what we observe, but is by no means consistent with random stacking ($\alpha=1$). Considering the limiting cases of ideal fcc and random stacking, only, the pore condensates of Brown *et al.* are closer to the former than to the latter case, in qualitative agreement with the present results.

As far as the evolution of the diffraction pattern with decreasing temperature is concerned, we have often produced diffraction patterns similar to that shown in Ref. 24 for Ar in Vycor at 37 K, but in our experiments the sharp component of the fcc peaks could be always removed by sufficiently long waiting or by pumping off small fractions of the total amount of gas in the cell. The patterns obtained after such treatments have no peculiar T dependence except shifts of the peaks due to thermal expansion and a slight increase of the intensities toward low T. The peak widths which are sensitive to stacking faults and size effects are independent of T down to 20 K.

IV. SUMMARY

The concept of adsorption and capillary condensation is well established by numerous experimental studies on van der Waals liquids in porous SiO_2 glasses. Our thermodynamic and structural study shows that the solid Ar condensate is also stable in the pores and undergoes a first-order transition from the adsorbate state into the capillary condensed state very much like the liquid. An analogous behavior can be expected for other van der Waals systems including the other rare gases, and also for H_2, CH_4, N_2, or CCl_4. Even though we have no indications for dewetting or any other phase transition in pore condensed Ar, dewetting may occur in other systems at lower temperatures, in particular in connection with subsequent structural phase transitions. In practice, it may be difficult to produce convincing evidence for a dewetting transition and to discriminate such a transition from the formation of the bulk solid in a nonequilibrium state because of the problem of slow kinetics at low T.

The adsorbate-substrate interaction calls for a layered structure of the pore material, and diffractometry has produced evidence that this is so. The first monolayer adsorbed crystallizes in a highly disordered triangular lattice. Further layers stack on the ones underneath, obeying the principle of spherical close packing. On capillary condensation, the crystals grow along the pore axis to a coherent linear extension of the order of several hundred Å. Altogether these results are not consistent with the naive view of the solidified material in the pores as fcc nanocrystals with an overall spherical shape, the size being given by the diameter of the pores.

The depression of the melting temperature is due to the fact that the reduction of the chemical potential of the pore condensate with respect to the bulk is larger in the liquid than in the solid state. We propose to relate the reduced stability of the solid capillary condensate to lattice defects, in particular stacking faults, which the solid has to form in order to adapt to the pore geometry. The solidification-melting hysteresis is due to the fact that the width of the adsorption-desorption hysteresis is larger in the solid than in the liquid

state. Presumably, the general features of the chemical-potential–temperature phase diagram established for the melting transition of Ar also apply for other phase transitions for which the pore condensate is in equilibrium with its vapor.

ACKNOWLEDGMENTS

This work has been supported by the Sonderforschungsbereich 277 ''Grenzflächenbestimmte Materialien.'' We thank D. Wallacher for helpful discussions.

[1] E. B. Molz, A. P. Y. Wong, M. H. W. Chan, and J. R. Beamish, Phys. Rev. B **48**, 5741 (1993).
[2] E. B. Molz and J. R. Beamish, J. Low Temp. Phys. **101**, 1055 (1995).
[3] J. R. Beamish, A. Hikata, L. Tell, and C. Elbaum, Phys. Rev. Lett. **50**, 425 (1983).
[4] C. L. Jackson and G. B. McKenna, J. Chem. Phys. **93**, 9002 (1990).
[5] D. G. Hendershot, D. K. Gaskill, B. L. Justus, M. Fatemi, and A. D. Berry, Appl. Phys. Lett. **63**, 3324 (1993).
[6] K. M. Unruh, T. E. Huber, and C. A. Huber, Phys. Rev. B **48**, 9021 (1993).
[7] R. Evans, U. M. B. Marconi, and P. Tarazona, J. Chem. Soc., Faraday Trans. 2 **82**, 1763 (1986).
[8] P. C. Ball and R. Evans, Langmuir **5**, 714 (1989).
[9] P. I. Ravikovitch, S. C. Ó. Domhnaill, A. V. Neimark, F. Schüth, and K. K. Unger, Langmuir **11**, 4765 (1995).
[10] W. F. Saam and M. W. Cole, Phys. Rev. B **11**, 1086 (1975).
[11] M. Schindler, A. Dertinger, Y. Kondo, and F. Pobell, Phys. Rev. B **53**, 11 451 (1996).
[12] J. Warnock, D. D. Awschalom, and M. W. Shafer, Phys. Rev. Lett. **57**, 1753 (1986).
[13] M. W. Maddox and K. E. Gubbins, J. Chem. Phys. **107**, 9659 (1997).
[14] G. B. Hess, *Phase Transitions in Surface Films 2*, edited by H. Taub, G. Torzo, H. J. Lauter, and S. C. Fain, Jr. (Plenum, New York, 1991).
[15] J. De Kinder, A. Bouwen, and D. Schoemaker, Phys. Rev. B **52**, 15 872 (1995).
[16] T. E. Huber and C. A. Huber, Phys. Rev. Lett. **59**, 1120 (1987).
[17] D. Wallacher, P. Huber, and K. Knorr, J. Low Temp. Phys. **111**, 419 (1998).
[18] P. E. Sokol, R. T. Azuah, M. R. Gibbs, and S. M. Bennington, J. Low Temp. Phys. **103**, 23 (1996).
[19] Y. Wang, W. M. Snow, and P. E. Sokol, J. Low Temp. Phys. **101**, 929 (1995).
[20] B. Schäfer, D. Balszunat, W. Langel, and B. Asmussen, Mol. Phys. **89**, 1057 (1996).
[21] B. S. Schirato, M. P. Fang, P. E. Sokol, and S. Komarneni, Science **267**, 369 (1995).
[22] D. W. Brown, P. E. Sokol, A. P. Clarke, M. A. Alam, and W. J. Nutall, J. Phys. C **9**, 7317 (1997).
[23] P. Huber and K. Knorr, J. Low Temp. Phys. **111**, 419 (1998).
[24] D. W. Brown, P. E. Sokol, and S. N. Ehrlich, Phys. Rev. Lett. **81**, 1019 (1998).
[25] A. W. Adamson, *Physical Chemistry of Surfaces* (Wiley, New York, 1990).
[26] B. E. Warren, Phys. Rev. **59**, 693 (1941).
[27] J. Z. Larese, Q. M. Zhang, L. Passell, J. M. Hastings, J. K. Dennison, and H. Taub, Phys. Rev. B **40**, 4271 (1989).
[28] B. E. Warren, *X-Ray Diffraction* (Addison-Wesley, Reading, MA, 1969).
[29] D. M. Zhu and J. G. Dash, Phys. Rev. B **38**, 11 673 (1988).
[30] J. G. Dash, Phys. Rev. B **25**, 508 (1982).